J Fail. Anal. and Preven. (2009) 9:370–379
DOI 10.1007/s11668-009-9256-8

TECHNICAL ARTICLE—PEER-REVIEWED

Failure Analysis of HAZ Cracking in Low C–CrMoV Steel Weldment

Nausheen Naz · Fawad Tariq · Rasheed Ahmed Baloch

Submitted: 12 September 2008 / in revised form: 24 April 2009 / Published online: 12 May 2009

Abstract This case study describes the failure analysis of steel nozzle in which cracking was observed after a circumferential welding process. The nozzle assembly was made from low C–CrMoV alloy steel that was subsequently single pass butt welded using gas tungsten arc welding. No cracks were found in visual inspection of the welds; however, X-ray radiography showed small discontinuous cracks on the surface in the area adjacent to weld bead, i.e. heat affected zone. The welding of nozzle parts made of same material was a routine process and this type of cracking did not occur in the past. Therefore, it became essential to determine the root cause of the failure. A detailed investigation including visual examination, nondestructive testing, optical microscopy, microhardness measurements and residual stress measurements were carried out to find out the primary cause of failure and to identify actions required to avoid its reoccurrence in future. Results of the investigation revealed that the principal cause of failure was the presence of coarse untempered martensite in the heat affected zone due to localized heating. The localized heating was caused by high welding heat input or low welding speed and resulted in the high transformation stresses. These transformation stresses combined with the thermal stresses and the constraint conditions to cause intergranular brittle fracture.

Keywords Nozzle · Heat affected zone · Weld cracking · Residual stresses · GTAW · Untempered martensite

N. Naz · F. Tariq (✉) · R. A. Baloch
Materials Research and Testing Laboratory, Pakistan Space and Upper Atmosphere Research Commission (SUPARCO), Karachi, Pakistan
e-mail: t_fawad@hotmail.com

Introduction

Low C–CrMoV steel is non-corrosion resistant high-strength steel widely employed for the applications demanding high strength combined with high toughness and good weldability in the treated condition. The tensile strength of this steel in annealed condition is 650–700 MPa and the strength rises to 1000–1180 MPa in treated condition. This makes the steel particularly suitable for large fabrications that require high strength and require that the welding of material in hardened-tempered condition [1]. The most important reason for the wide applicability of CrMoV steel is that it can be satisfactorily joined by a variety of welding processes. No pre- or post-weld heat treatment is required and machining of the steel in either the annealed or treated state does not generate any particular difficulties. Common applications include manufacturing of pressure vessels, aircraft components, booster motors, etc.

Because of its availability, high specific strength and comparatively simple heat treatment, 0.1%C–1.25%Cr–0.8%Mo–0.2%V steel was selected for the fabrication of a nozzle assembly that required welding. Convergent and ring halves of the steel that were about 2.6 mm thickness were butt joint in treated condition using filler wire of similar composition by gas tungsten arc welding to form single nozzle assembly. No post-weld heat treatment was employed. In general, defect-free, high-quality welds can be obtained by GTAW in this steel. However, in this case small cracks were detected by radiography and dye penetrant testing in the vicinity of the weld metal after welding. These cracks were not observed during visual inspection. At this stage it was not confirmed that whether cracks were produced during welding or formed after welding and therefore the cracking could not be specifically associated

with either hot cracking or cold cracking. Since cracking usually did not occur in routine practice a failure analysis became essential in order to find the root cause of failure. The investigation into the possible reasons responsible for weld failure included a study of the various metallurgical and/or process parameters likely to cause this failure as well as evaluation of the failed component.

Visual Examination, Non-Destructive Testing and Collection of Data

The nozzle assembly was made of low carbon Cr–Mo–V alloy steel sheet having a thickness of 2.6 mm. Sheets to be welded were austenitized at 975 °C and air cooled. Tempering was done at 625 °C for 30–45 min followed by air cooling. Parts were single pass butt welded after machining to required dimensions using gas tungsten arc welding process and filler wire of the similar composition as that of steel sheet. Argon gas of 99.99% purity was used for shielding. No further heat treatment was carried out after welding.

No cracks were observed in the weld joint and adjacent area during visual inspection after welding. However, radiography of the whole part revealed some cracks adjacent to the weld bead as shown in Fig. 1. This type of weld cracking had not been experienced in past using same process parameters. Therefore, a thorough investigation was carried out in order to collect as much information as possible in an attempt to establish the cause of cracking. In the first step, dye penetrant techniques were used to reveal the cracks and for subsequent crack measurements. It was observed that cracks were not present in the weld bead rather they initiated in the area adjacent to the weld zone, i.e. in the heat affected zone (HAZ) and propagated toward the base metal with an angle roughly 30° to the weld zone, as shown in Fig. 2. Furthermore, cracks were not continuous; they are lying intermittently and initiated independently of each other. The overall length of the cracked region as revealed by the DP was found to be 33 mm.

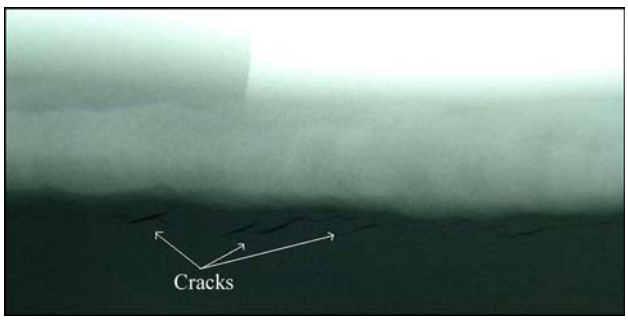

Fig. 1 Radiograph of welded part showing cracks adjacent to the weld bead

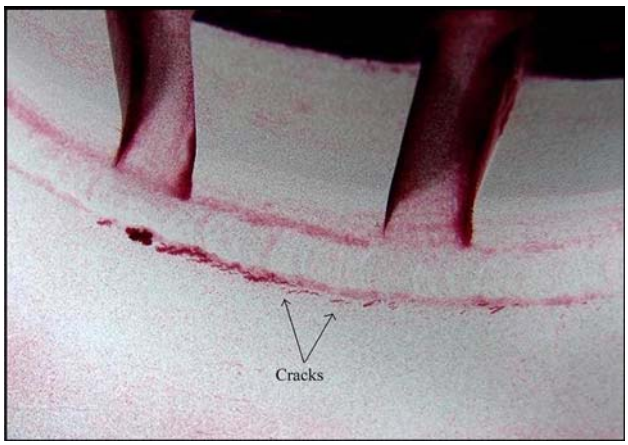

Fig. 2 Location and morphology of cracks as revealed by dye penetrant testing

Table 1 Welding parameters used to weld nozzle assembly

Welding voltage, V	Welding current, A	Feed speed, mm/min	Carraige speed, rpm	Gas flow rate, m^3
12.2–12.6	90–96	32–36	34–38	16

The quality of the weld is partially governed by the quality of the weld metal (fusion zone) and HAZ. Major welding parameters that affect the quality of the weld are specific heat input, number of passes, inter-pass temperature, pre-heating, post-heating, electrode diameter and restraint during welding. Table 1 summarizes the main welding parameters used to obtain the joint.

Spectroscopy

Spectroscopic analysis of the failed part and weld bead was carried out in order to find out the actual chemical composition of the steel part and filler metal for comparison with the specified chemical composition. Table 2 shows the recommended and actual chemical composition of the steel nozzle and filler wire.

Residual Stress Measurements

Residual stresses are often introduced unintentionally during fabrication—for example, during welding or heat treatment. In weld joints, they arise as a consequence of the heterogeneous application of energy and localized fusion. The magnitude of these stresses depends on the welding parameters like joint thickness and configuration, heat input, cooling rates, constraint conditions, etc. [2]. In many cases, residual stresses are detrimental to material performance in the sense that they affect the load bearing

Table 2 Recommended and actual chemical composition (in wt.%) of steel nozzle assembly and filler metal

	C	Si	Mn	P	S	Cr	Mo	V
Recommended chemical composition								
Nozzle assembly	0.10–0.16	≤0.20	0.8–1.1	≤0.020	≤0.015	1.25–1.50	0.8–1.0	0.20–0.30
Filler metal	0.11	≤0.20	1.0	≤0.020	≤0.015	1.40	0.90	0.25
Actual chemical composition								
Nozzle assembly	0.14	0.16	0.94	≤0.020	≤0.015	1.26	0.8	0.24
Filler metal	0.10	0.18	0.87	≤0.020	≤0.015	1.31	0.87	0.25

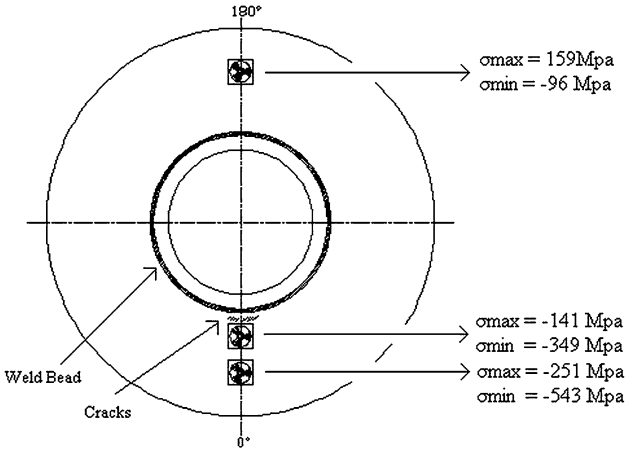

Fig. 3 Schematic of the nozzle assembly showing location of the strain gages along with the value of max and min principal residual stresses

capability of the material. Hence, it becomes essential to measure any locked-in stresses stored in the material after welding process. Residual stress measurement was carried out on welded part using hole drill method as per ASTM standard E 837. Electric resistance-type strain gage rosettes of 120 Ω of 5.13 mm diameter were used for this purpose. Attention is given to the area adjacent to the weld bead where cracks were observed. Locations of the rosette along with the values of principal stress are shown in Fig. 3.

Fractography

A section of the cracked surface was carefully opened for the identification of fracture mechanism. Fractography was then carried out using stereomicroscope at the magnification of 15× and 50×. Results of the fractography are shown in Fig. 4 and 5, respectively.

Macro-examination

Samples were sectioned from the region containing cracks for macro-examination. Transverse face and capping face both were grinded up to 400 grit size and etched in 2% nital

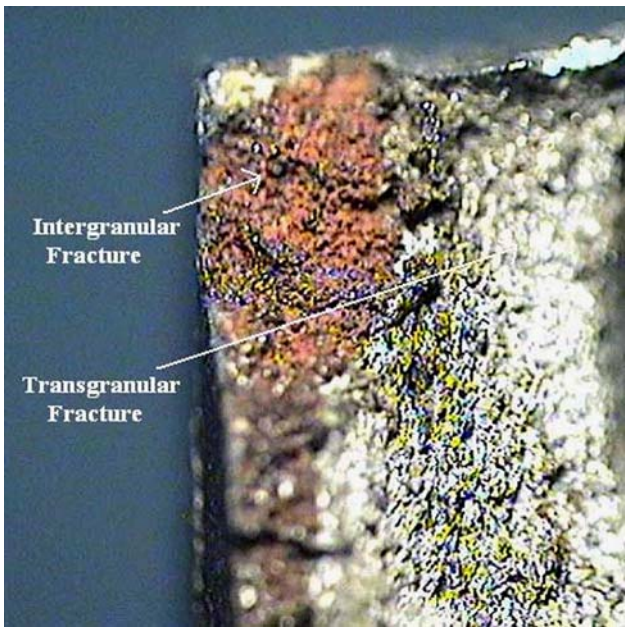

Fig. 4 Fractographs showing intergranular and transgranular mode of fracture after carefully opening the cracked surface (magnification 15×)

to reveal different regions of the weldment. Special care was taken to avoid excessive heating of required surface during grinding. Figure 6 shows the macrograph of the transverse face after etching. Note that the oxidized surfaces demonstrate that cracking occurred while the weld was hot.

Microstructure Observations

Micro-examination of both transverse and capping surfaces of the specimen containing cracks was also conducted in order to reveal phases produced in different zones of the weld and to observe the cracks on micro level. Furthermore, a specimen was also sectioned from the area adjacent to the weld bead having no cracks and prepared for micro-examination for comparison. Both transverse face and capping face of the each sample were prepared for micro-examination by conventional grinding and polishing technique and etched in 2% nital solution for optical microscopy.

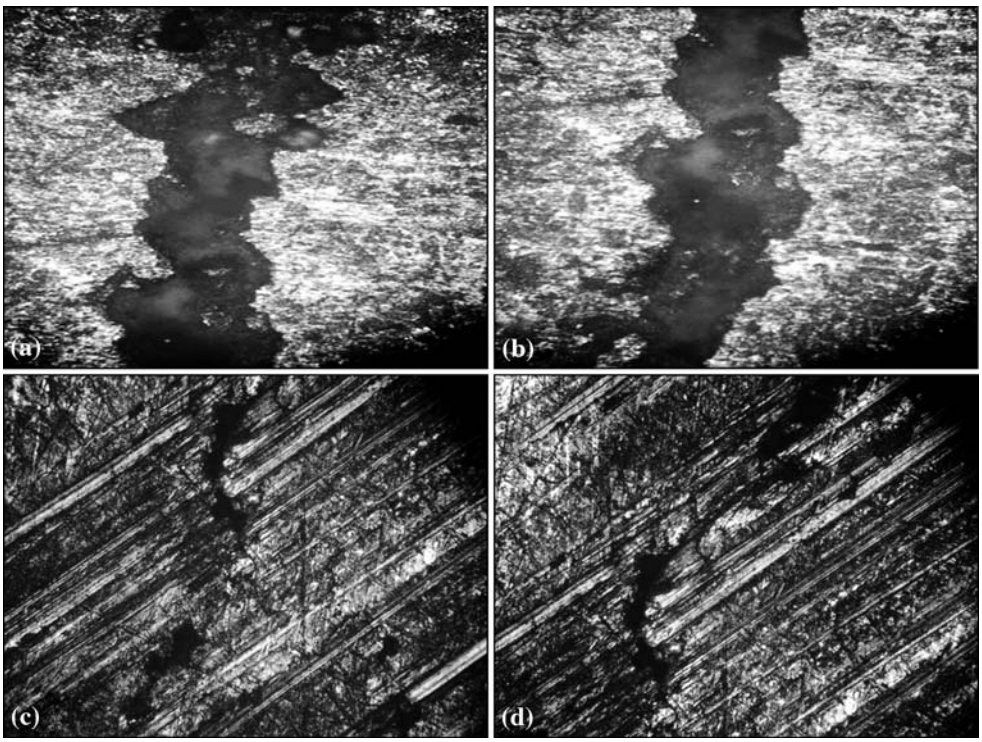

Fig. 5 Fractographs of cracked region showing cracks in the HAZ (**a**, **b**) on transverse face and (**c**, **d**) on the surface of the sheet (magnification 50×)

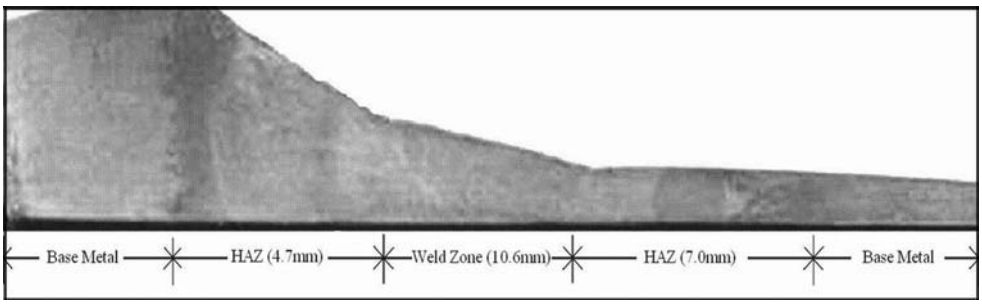

Fig. 6 Different zones produced in transverse face after single pass gas tungsten arc welding along with relative sizes of zones

Microstructures produced in different regions of the capping face of un-cracked specimen and transverse face and capping face of cracked specimen are shown in Fig. 7, 8, and 9, respectively.

Figure 10 shows the high magnification (1000×) optical micrographs of the cracks revealing fine details of the matrix structure as well as the crack morphology.

In addition to micro-examination, the ASTM grain size number for different zones produced in the weld joint of cracked and reference un-cracked specimens was also calculated using image analysis software and the results are shown in Table 3.

Microhardness Measurements

Microhardness measurements were carried out on sample containing cracks and on sample without any crack using Vickers microhardness tester using 500 g load at a magnification of 500×. Figures 11 and 12 show the microhardness values in different regions of weldments.

Discussion

From NDT of failed part, cracks were found to be located in the HAZ of the weldment as shown in Fig. 1 and 2. In the first instance, it was thought that this was a type of cold cracking since this type of HAZ cracking is usually found to be produced after welding and attributed to nascent hydrogen diffusing into the joints during welding [3]. This embrittle the material resulting cold cracking. Common sources of hydrogen pickup are welding electrodes, shielding materials, organic compounds, moisture, surrounding atmosphere, etc. [3]. In order to check the possibility of hydrogen pick-up during welding, storage

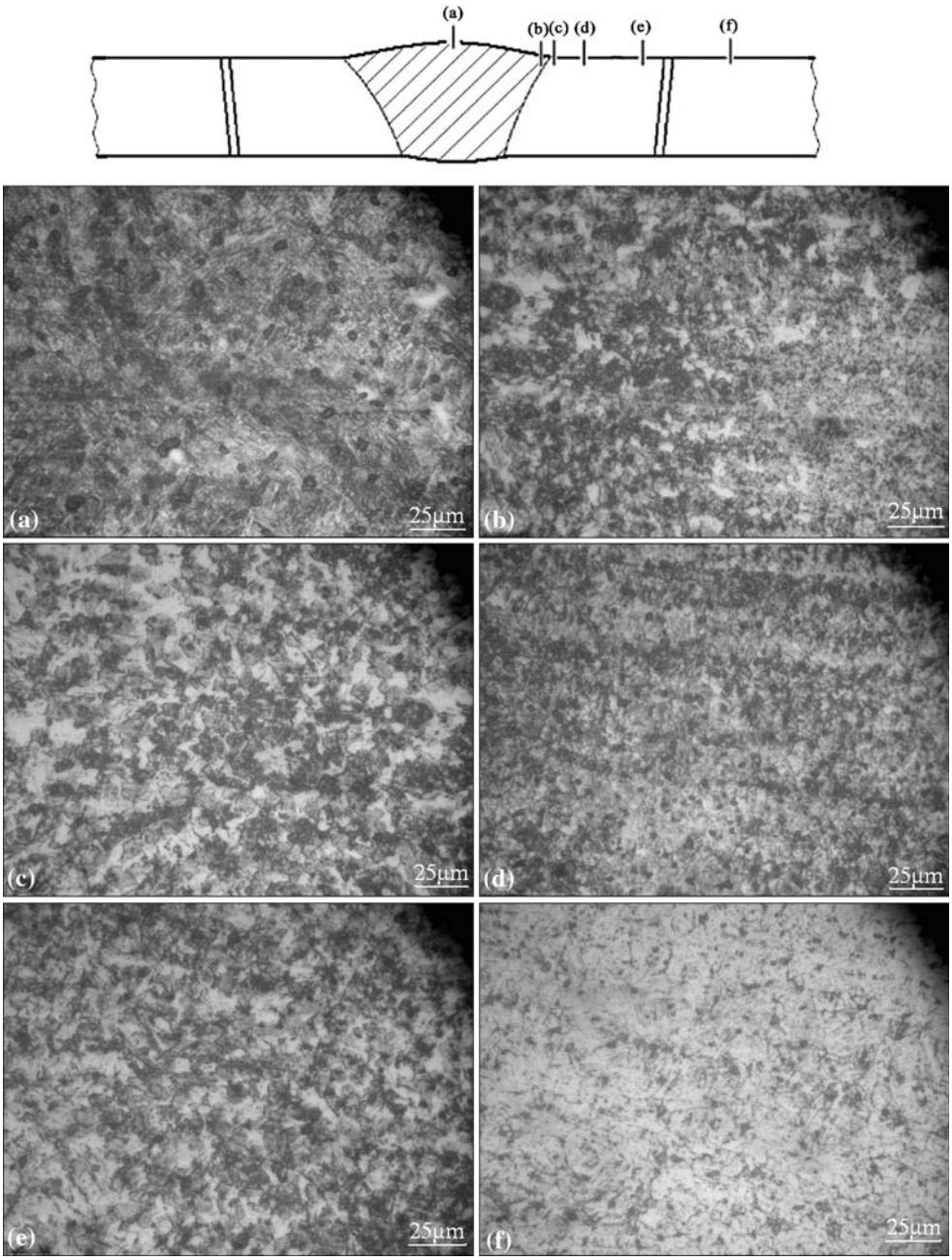

Fig. 7 Optical micrographs of un-cracked specimen showing (**a**) weld zone, (**b**) fusion boundary, (**c**) coarse grained HAZ, (**d**) fine grained HAZ, (**e**) intercritical HAZ and (**f**) base metal (magnification 200×)

conditions and quality of filler wires were examined and found satisfactory. Furthermore, it was also confirmed that joint was properly cleaned and dried before welding. Hence, there were very little chances of hydrogen pickup during welding.

From the result of spectroscopy as shown in Table 2, it was observed that there was no significant departure in the composition of either nozzle assembly or filler wire from the recommended compositions. Welding parameters used to weld this nozzle assembly are given in Table 1 and found to be in compliance with the recommended parameters. Furthermore, welding of similar nozzle assembly using same welding parameters and restraint conditions was a routine practice and produced defect-free joints in past.

From the result of residual stress measurements near cracked region, in region away from crack and opposite side of the weld bead having no cracks gave an idea that there were no significant stresses produced during welding. Maximum value of tensile residual stress was found on the opposite side of the cracked region away from weld bead, i.e. 159 MPa as shown in Fig. 3.

Fractrography of the weldment, containing cracks, subsequent to sectioning revealed intergranular mode

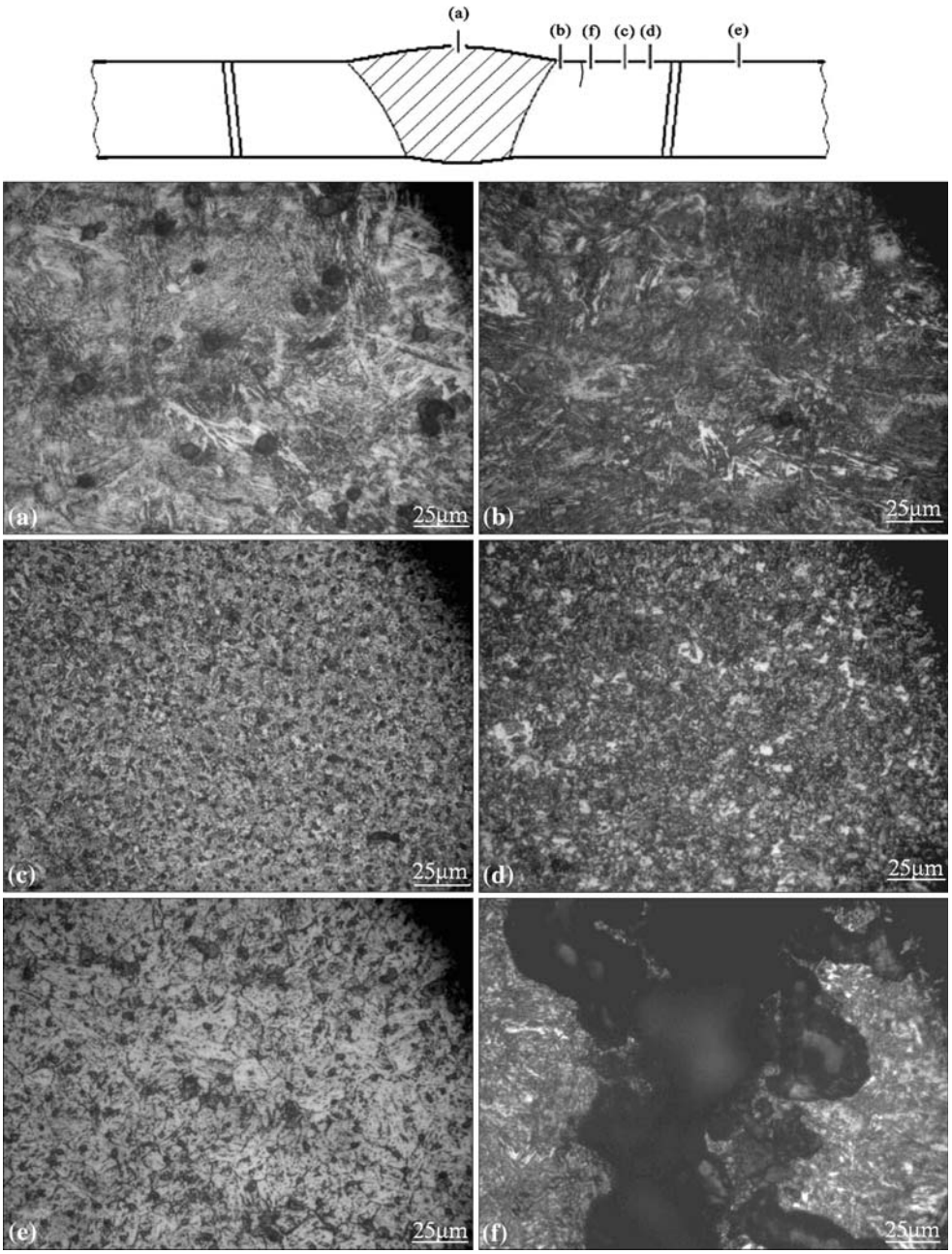

Fig. 8 Optical micrographs of transverse face of cracked specimen showing (**a**) weld zone, (**b**) coarse grained HAZ, (**c**) fine grained HAZ, (**d**) HAZ, (**e**) base metal and (**f**) cracks in coarse grained HAZ (magnification 200×)

of fracture in the HAZ as seen in reddish color in Fig. 4. The crack propagated along the grain boundaries to the depth of approximately 0.8 mm. This type of intercrystalline fracture usually occurs when the phase in the grain boundary is weak and brittle. Grain boundary cracking can also occur as a result of quench cracking in hardened and tempered steel. Other sources of grain boundary cracking are elevated temperature stress rupture condition, in the presence of impurity at grain boundaries and in the presence of hydrogen and liquid metals on grain boundaries [4]. In steel especially, intergrannular fracture is frequently caused by hydrogen embrittlement or hydrogen-assisted cracking. However, the chances of hydrogen pickup in this case during welding were very low because of argon gas shielding. Also, filler wires used for welding were coated to avoid hydrogen absorption. Detailed investigation of the remainder of the fracture surface under stereomicroscope, where cracking was not occurred, revealed that the fracture mode was predominantly transgranular cleavage with some limited areas of dimple rupture (bright, shiny flat surface in Fig. 4). Figure 5 shows the location of the cracks, its propagation path and morphology at comparatively higher magnification (i.e. 50×) from which no evidence of single or multiple sources for fracture initiation was observed.

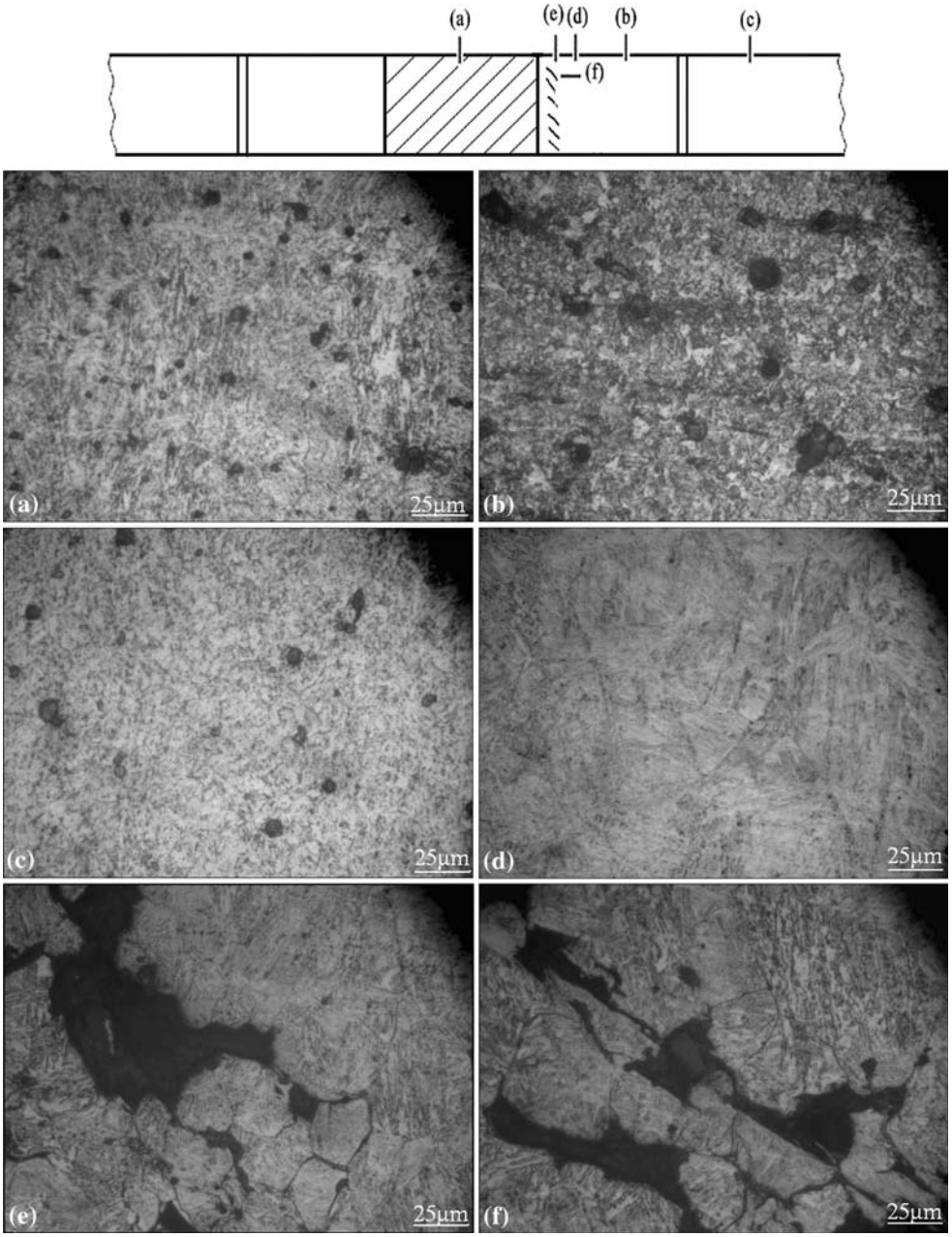

Fig. 9 Optical micrographs of capping face of cracked specimen showing (**a**) weld zone, (**b**) HAZ, (**c**) base metal, (**d**) CGHAZ and (**e**) intergranular cracks in CGHAZ and (**f**) intergranular cracks and grain boundary decohesion in CGHAZ (magnification 200×)

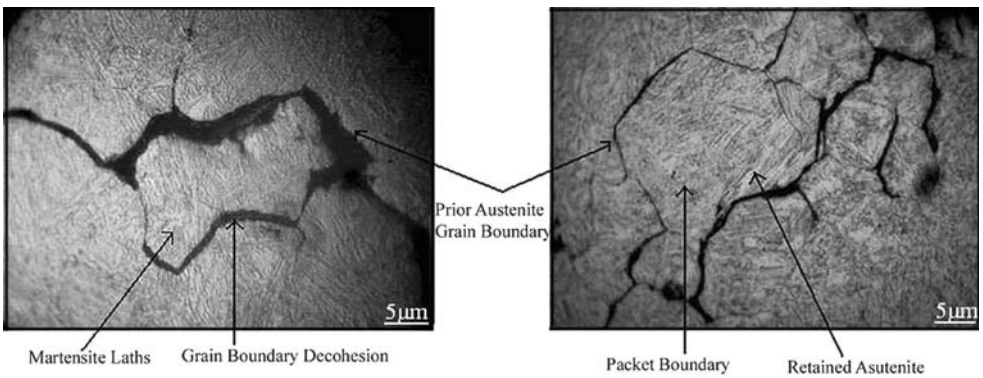

Fig. 10 Optical micrographs showing typical lath martensitic structure with grain boundary decohesion at prior austenite grain boundaries (magnification 1000×)

Table 3 ASTM grain size number for various zones in weld joint

Zone	ASTM grain size no.	
	Un-cracked specimen	Cracked specimen
Weld zone	8–8.5	8–8.5
HAZ (coarse grained)	7.7–8	6–6.5
HAZ (fine grained)	8.5–9	8.5–9
Base metal	8.5–9	8.5–9

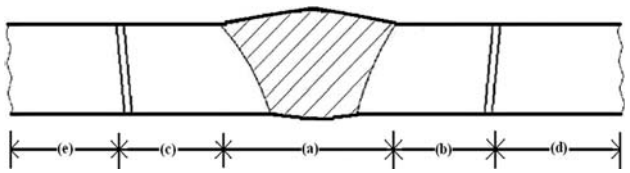

Fig. 11 Microhardness values in different zones of weld joint as taken on reference specimen, i.e. without cracks, are (a) weld zone 345–355 HV, (b) HAZ 357–367 HV, (c) HAZ on opposite side of weld bead 353–367 HV, (d) base metal 346–357 HV and (e) base metal on opposite side of weld bead 347–358 HV

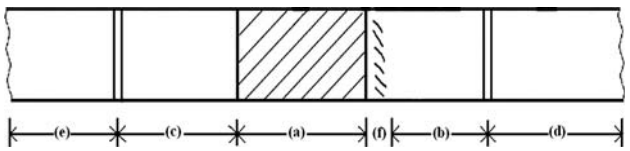

Fig. 12 Microhardness values in different zones of weld joint of specimen containing cracks are (a) weld zone 350–360 HV, (b) HAZ 360–370 HV, (c) HAZ on opposite side of weld bead 360–370 HV, (d) base metal 345–355 HV, (e) base metal on opposite side of weld bead 350–360 HV and (f) region containing cracks 380–390 HV

From the results of macro-examination, it was observed that the cracks were confined to the HAZ of the weldment and were discontinuous and spread at an area of approximately 33 mm. Cracks were not found to be propagated to the entire thickness of the sheet, rather they ceased at the depth of around 0.82 mm. It was further observed that the HAZ produced as a result of welding on the side where cracks were found was wider as compared to the HAZ produced on the other side of the weld zone because of thickness variation in both sheets and the resulting thermal gradient, as seen in Fig. 6. Furthermore, it was found that the HAZ containing cracks was larger approximately 7 mm than the adjacent crack-free HAZ, i.e. approximately 6 mm. As the size of the HAZ is primarily controlled by the magnitude of the weld heat input, therefore it seems that the increase in the size of the cracked HAZ was the result of either increased weld heat input or low welding speed causing localized heating.

Microscopic study on reference un-cracked and cracked weldments revealed three distinct regions which are the characteristic of low alloy steel weld joints: weld zone (WZ), HAZ and base metal (BM) as shown in Fig. 7, 8 and 9, respectively. Figure 7(a) shows the WZ (i.e. fusion zone), which is the region where the peak temperature exceeds the melting point of BM. Microstructure produced in the WZ of all specimens consists of bands of tempered martensite with coarse spheroid cementite at the boundaries as seen in Fig. 7(a), 8(a) and 9(a). Figure 7(b) shows the fusion boundary (transition zone) which separates WZ from adjacent HAZ. Adjacent to the WZ is a HAZ; a region that is not heated sufficiently to cause melting, but nevertheless the microstructure is altered by the heat input during welding. Because the thermal conditions vary with distance from the fusion line, the HAZ can be further divided into three zones according to the extent to which grain growth and austenitization occur; into a coarse grained HAZ (CGHAZ), a fine grained HAZ (FGHAZ) and intercritical HAZ (IGHAZ). Figure 7(c) shows the CGHAZ of the reference un-cracked specimen as observed from the capping surface. Since this zone is located adjacent to the weld zone, it was heated to high temperatures (above Ac_3). Consequently, the austenite that formed was annealed during heating beyond Ac_3, giving rise to a coarse grain structure. Microstructure of the CGHAZ in this case is a mixed structure consisting mainly tempered martensite with some amount of pearlite as shown in Fig. 7(c). Moving away from the CGHAZ toward the BM is the FGHAZ that was not heated beyond Ac_3 temperature. Its microstructure is similar to that produced in CGHAZ but of finer grain size as shown in Fig. 7(d) and 8(c). Figure 7(e) shows the IGHAZ that was partially austenitized during the heating part of the thermal cycle. The part that does not transform into austenite becomes tempered. Microstructure in this zone consists of refined ferrite and pearlite with minor amount of tempered martensite as seen in Fig. 7(e). Figures 7(f), 8(e) and 9(c) show the microstructures produced in the BM of un-cracked and cracked specimen and consist mainly of fine equiaxed pearlite with some ferrite. Table 3 shows the grain size number measured in different regions of the weld joint. It was observed from Table 3 that the grain size number of WM is 8–8.5 whereas that of FGHAZ and BM is 8.5–9 for both cracked and un-cracked reference specimens.

From microscopy of both cracked and un-cracked specimens it was found that the microstructures produced in all zones of the weldment are similar except that produced in that of CG HAZ of cracked specimen. Figures 8(f) and 9(d) show the micrographs of CGHAZ as seen from transverse face and capping face. It consists of coarse grains of lath martensite which was not tempered during subsequent cooling rather than tempered martensite which was seen in CGHAZ of un-cracked specimen. In addition to this, it was also observed that the grain size number in CGHAZ of cracked specimen is 6–6.5, which is less than 7.7–8 produced in CGHAZ of un-cracked specimen as given in

Table 3. This increase in the grain size in CGHAZ of cracked specimen showed that this zone was heated to very high temperatures, i.e. in excess of 1200 °C, causing the substantial growth of the austenite grains, which subsequently transform to the martensite on cooling. The reason for this abnormal grain growth in our opinion was either the increase in the welding heat input or low welding speed resulting in the rise of the temperature in CGHAZ, thus producing coarse prior austenite grains, which on subsequent cooling to room temperature formed untempered martensite as shown in Fig. 9(d).

Figure 8(f) shows the micrograph of the crack in CGHAZ of cracked weldment as seen on transverse face, whereas Fig. 9(e) and (f) shows the intergranular cracks and grain boundary decohesion in the CGHAZ as seen on capping face. From the micrographs taken at higher magnification it was revealed that the crack followed the intergranular path, i.e. along the prior austenite grain boundary (Fig. 10). Furthermore, the zone where cracks were found was very coarse and consists of un-tempered martensite with some regions of retained austenite in between martensite laths as shown in Fig. 10. The cracks were found only in the CGHAZ and occurred by grain boundary decohesion, giving a fracture surface that resembles a low-temperature brittle fracture. Normal mode of fracture in low C–CrMoV steel is transgranular, but in this case, the fracture was found to be brittle intergranular which indicates that the grain boundaries were weakened due to some reason [5]. Main source of grain boundary weakening in low alloy steels is segregation of P, S, As, Sb, Sn, etc., to the prior austenite grain boundaries. But the steel under study was very low in P, S, and other harmful impurities. Furthermore, careful examination at higher magnification also did not show any evidence of segregation. However, the chances of solute atom segregation cannot be completely neglected because the diffusion of solute atoms toward grain boundaries is accelerated at higher temperatures. Also, embrittling effect of harmful segregating species is significantly increased with the increase in the grain size of the material because coarse grain size provides shorter grain boundary length or surface area of grains per unit volume to accommodate the segregating harmful species. Such segregation decreases the interfacial cohesive strength and changes the brittle fracture mode from a typical transgranular cleavage fracture to intergranular decohesion [6].

The main hazard in welding is the formation of martensite in the HAZ, near the weld, which can readily lead to microcracks. In welding, it is therefore essential to have steel with a low carbon equivalent (CE) which is an important indicator of the hardenability of HAZ. Alloys containing carbon $\geq$0.4 wt.% show a tendency to form martensite on welding and therefore are considered difficult to weld [7]. It is therefore necessary to limit the carbon content below 0.4% for heavy structural steels; if it is greater than this, controlled cooling of the weld is necessary to avoid risks of embrittlement. In order to find the reason for martensite formation in HAZ, the CE of the steel used in this study was calculated using empirical formula given by Ito and Besseyo [8] and found to be 0.33. At this value of CE, steel is considered to be safe in regard of formation of martensite in HAZ on welding. However, martensite can be produced in the weldment if the part is rapidly cooled.

$$\begin{aligned} \mathrm{CE} = {} & \mathrm{C} + (1/30)(\mathrm{Si}) + (1/20)(\mathrm{Mn} + \mathrm{Cu} + \mathrm{Cr}) \\ & + (1/60)(\mathrm{Ni}) + (1/15)(\mathrm{Mo}) + (1/10)(\mathrm{V}) \\ & + 5\mathrm{B}\ \text{wt.}\% \end{aligned}$$

But in this case, untempered martensite was found in CGHAZ, which should not be produced as showed from the calculation of CE. The formation of untempered martensite thus needs explanation. An important reason for the formation of martensite in the CGHAZ is the coarse prior austenite grain size. The coarse prior austenite grain size produced at higher temperatures (due to localized heating) has higher hardenability as compared to fine grain sizes, because the grain boundary area per unit volume decreases. This results in lesser number of potent sites available for nucleation of ferrite and pearlite. Thus, the transformation of austenite into softer phases (i.e. ferrite-pearlite) is slowed down with the increase in the tendency for martensitic transformations and the hardenability therefore increases. This increase in hardenability is responsible for the transformation of austenite into martensite even under the conditions of slow cooling. The coarse microstructure produced is therefore higher in hardness as compared to fine microstructure in case of weld structures but the strength and ductility of coarse grained microstructure goes down. Grain boundaries of the coarse microstructure became weak as compared to the fine microstructure. This trend in hardness was also confirmed by the microhardness measurements on both un-cracked and cracked weld joints as shown in Fig. 11 and 12 respectively.

From Fig. 11, hardness was found to be similar in WZ and BM, i.e. $\sim$345–355 HV, whereas hardness of CGHAZ and FGHAZ on both sides of the WZ was $\sim$357–367 HV. Somewhat similar hardness values were observed in different zones of cracked weldment except in the region containing cracks, i.e. CGHAZ. In CGHAZ containing brittle intergranular cracks, hardness was 380–390 HV which confirms the presence of untempered martensite, which was the result of higher hardenability of coarse grains.

On the basis of fractography and microscopic examination, the principal cause of brittle intergranular cracking

in HAZ of weldment was weakening of grain boundaries due to grain coarsening at higher temperatures because of high welding heat input or low welding speed at this area which causes localized overheating, the resulting coarse austenite on subsequent cooling to below M_s transformed to brittle untempered martensite. This has induced transformation stresses which were tensile in nature (due to volume change from austenite to martensite) in the region. In addition to this, thermal stresses arising from rapid heat transfer from regions of high temperature to surrounding mass of low temperature and different cooling rates experienced by the surface and the interior of the steel and the stress induced by the constraint conditions (due to welding fixture) all together resulted in increase in the stress to a level greater than fracture stress for intergranular fracture. It is further concluded that the cracking observed in HAZ of the weldment is a type of hot cracking (i.e. cracking which occurs at elevated temperature during welding) rather than cold cracking and the reason for this is that the cracks were found to be produced in martensitic phase in CGHAZ and the martensite start temperature (M_s) of this steel is estimated to be in the range 415–428 °C using empirical relations formulated by Andrews [9] and Barralis and Maeder [10]. The cracks were therefore thought to be initiated during welding which then propagated along the grain boundaries of coarse grained brittle martensite on subsequent cooling to room temperature.

The confinement of the cracking to the HAZ of the weldment and no observable damage in the other zones of the weld joint, along with the absence of inclusions, second phase particles or hydrogen pickup therefore suggest that the main cause of failure was the stresses developed as a result of martensitic phase transformation combined with thermal and constraint conditions imposed during welding.

Conclusions

The results of the investigation carried out on failed weldment of low C–CrMoV steel led to the following conclusions:

1. The fractography of the fracture surface indicated the brittle intergranular mode of fracture. These cracks were confined only in the HAZ of the weldment and appeared to propagate with an angle toward the base metal.
2. Metallographic examinations of the fracture revealed that cracks were produced in the CGHAZ, consisting of coarse grains of untempered martensite, which was the result of localized overheating of this zone due to either high weld heat input or low welding speed. Additionally, the coarse grained martensite significantly reduced the strength and ductility of the HAZ.
3. The stresses developed due to transformation of austenite to brittle untempered martensite combined with thermal stresses (due to temperature gradient) and constraint conditions during welding lead to brittle intergranular fracture of the weldment.

Acknowledgments This failure analysis was carried out in the Materials Research and Testing Laboratory of Pakistan Space and Upper Atmosphere Research Commission (SUPARCO). The authors wish to thank Mr. Muhammad Saraf (Deputy Chief Manager) and Dr. Sajid Mirza (Senior Chief Manager) for their valuable suggestions and Mr. Raza Hussain (Chairman SUPARCO) for his guidance and provision of facilities throughout this investigation. The authors also like to thank Mr. Badar-ul-Hassan (Technical Officer) for his technical assistance throughout the experimental work.

References

1. Kishore Babu, N., Suresh, M.R., Sinha, P.P., Sarma, D.S.: Effect of austenitizing temperature and cooling rate on the structure and properties of a ultrahigh strength low alloy steel. J. Mater. Sci. **41**, 2971–2980 (2006)
2. Francis, J.A., Bhadeshia, H.K.D.H., Withers, P.J.: Welding residual stresses in ferritic power plant steels. J. Mater. Sci. Technol. **23**, 1009–1020 (2007)
3. Blodgett, O.W., Scott Funderburk, R., Miller, D.K., Quintana, M.: The Fabricators' and Erectors' Guide to Welded Steel Construction, pp. 42–44. The James F. Lincoln Arc Welding Foundation (1999)
4. McMahon, C.J., Jr.: Brittle fracture of grain boundaries. Interface Sci. **12**, 141–146 (2004)
5. Islam, M.A.: Grain boundary segregation behavior in 2.25Cr-1Mo steel during reversible temper embrittlement. J. Mater. Eng. Perform. **16**, 73–79 (2007)
6. Low, J.R., Jr.: In Relation of Properties to Microstructure, p. 163. ASM, Cleveland, OH (1954)
7. Suresh, M.R., Sinha, P.P., Sarma, D.S., Ballal, N.B., Krishna Rao, P.: Study of welding characteristics of 0.3C–CrMoV(ESR) ultrahigh strength steel. J. Mater. Sci. **42**, 5602–5612 (2007)
8. Bhadeshia, H.K.D.H., Honeycomb, R.: Steels: Microstructure and Properties, 3rd edn., pp. 296–297. Elsevier (2006)
9. Andrews, K.W.: Empirical formulae for the calculation of some transformation temperatures. J. Iron Steel Inst. **203**, 721–727 (1965)
10. Barralis, J., Maeder, G.: Métallurgie Tome I: Métallurgie Physique, Collection Scientifique ENSAM, p. 270 (1982)